JOURNAL OF GUIDANCE, CONTROL, AND DYNAMICS
Vol. 23, No. 6, November–December 2000

Identification and Control of Limit Cycle Oscillations in Aeroelastic Systems

Thomas W. Strganac,* Jeonghwan Ko,† and David E. Thompson‡
Texas A&M University, College Station, Texas 77843-3141
and
Andrew J. Kurdila§
University of Florida, Gainesville, Florida 32611-6250

Nonlinearities in the aeroelastic system induce pathologies such as the observed store-induced limit cycle oscillations found with certain high-performance aircraft configurations. Many previous studies, including efforts by these authors, focus on the nonlinear behavior of the uncontrolled, nonlinear aeroelastic system. These studies are briefly reviewed. However, there is limited study of the active control of these nonlinear aeroelastic systems. Although a linear controller may stabilize the nonlinear system under some circumstances, empirical evidence suggests that these control methods will prove unreliable in strongly nonlinear regimes and that stability is not guaranteed. The development of control strategies appropriate for these nonlinear systems are described. A nonlinear controller and the resulting closed-loop stability based on a partial feedback linearization are discussed. The approach depends on the exact cancellation of the nonlinearity. Hence, an adaptive control method is introduced in which guarantees of stability are studied. Experimental results obtained using the adaptive control system are presented.

Introduction

FLIGHT tests of several advanced high-performance aircraft have revealed nonlinear aeroelastic responses within their flight envelopes. For example, several aircraft models have experienced store-induced limit cycle oscillations (LCOs) for certain attached wing store configurations (see Refs. 1–3). Many studies have established that aeroelastic systems are inherently nonlinear and that these nonlinearities lead to phenomena not properly described by linear representations. For example, multivalued responses that lead to jump phenomena, limit cycles, modal interactions, and various types of resonances (internal and super/subharmonic) may result. Sources of nonlinearities include inertial (due to the location of concentrated or distributed masses), aerodynamic (due to dynamic stall, large oscillations leading to flow separation, oscillating shocks, or other unsteady flow sources), and structural (due to damping mechanisms, materials, large deflections, or partial loss of structural or control integrity).

The underlying physical mechanism that leads to nonlinear instabilities such as store-induced LCOs is not well understood, but it is well established that these nonlinearities have significant effects on aeroelastic stability and that these nonlinearities must be considered for the accurate prediction and active suppression of the associated instabilities. With advances in analytical and computational technologies providing accurate analysis of the dynamics and stability of such vehicles, there has been much recent study in nonlinear aeroelasticity. An excellent review of these advances may be found in Refs. 4 and 5.

Although aerodynamic nonlinearities may induce nonlinear responses, and significant progress has been made in this area, many investigations suggest that structural nonlinearities must be considered. In fact, stiffness tests conducted on some aircraft show evidence of a spring-hardening nonlinearity in the wing torsional mode. Whereas this phenomenon merits further study, it is a reasonable conjecture that this type of nonlinearity may lead to LCO behavior similar to that described herein.

Structural nonlinearities become evident as free-play, hysteresis, and hardening or softening stiffness in the bending or torsional modes of a wing. An extensive review of the analysis of structural nonlinearities for a wing section, such as that discussed in this paper, may be found in Lee et al.[6] who present extensive bifurcation analysis and necessary background theories for the analysis. Several recent investigations examine the response due to free-play or deadband nonlinearities.[7–10] Analytical studies on continuous nonlinear structural stiffness effects, such as those exhibited by the response of high-aspect-ratio thin wings, helicopter rotor systems, or propeller systems subjected to large torsional amplitudes, have been addressed by several researchers (see Refs. 8 and 11–15) but only Tang and Dowell[11,12] have experimental studies of systems in which continuous nonlinear stiffness behavior has been reported.

In Ref. 7, an experimental investigation of freeplay nonlinearities in a control surface is presented, and in Refs. 8–10 a bifurcation analysis of a wing section with freeplay nonlinearities is presented. Several studies address smooth (continuous) classes of nonlinearities that may be expressed in terms of cubic or higher-order polynomials; some recent studies include the work in Refs. 6, 8, and 15–18. In Ref. 16, analytical predictions are compared to experimental measurements for continuous nonlinear stiffening behavior in the pitch mode. Most important, the existence of LCO behavior is found for systems that exhibit nonlinear stiffness nonlinearities. These nonlinearities lead to LCOs that are dependent on velocity and the nonlinear parameters. It is shown for cases with continuous nonlinearities that the limit cycle motion consists of many higher harmonic components in addition to the dominant flutter frequency.

Observations from ground- and flight-test measurements of the F-16 (Refs. 1 and 2) and the F/A-18 provide motivation for further study. These observations include 1) stiffness tests that show evidence of a spring-hardening type of nonlinearity in the wing torsional stiffness and measurements that show that the wing behaves differently for leading-edge down vs leading-edge up; 2) LCOs that may be triggered by angle of attack (AOA); 3) LCOs that occur as low as $M = 0.6$ at elevated AOA; and 4) LCOs that are sensitive to the tip missile configuration.

Furthermore, results obtained from wind-tunnel investigations[19] of aeroelastic behavior indicate a signature of response similar to

Received 9 March 1999; revision received 25 October 1999; accepted for publication 29 October 1999.

*Associate Professor, Department of Aerospace Engineering. Associate Fellow AIAA.
†Postdoctoral Research Associate, Department of Aerospace Engineering. Member AIAA.
‡Graduate Research Assistant, Department of Aerospace Engineering. Student Member AIAA.
§Associate Professor, Department of Aerospace Engineering, Mechanics, and Engineering Science. Member AIAA.

that found in the LCO response of store configurations. While performing routine investigations to identify the aeroelastic stability boundary of a new wing configuration with external devices, an unexpected response, when compared with predictions from computational methods based on linear theory, occurred during wind-tunnel tests. Limit cycle flutter was observed much lower than linear analysis had predicted for classical flutter. The observed vibration characteristics suggested the presence of internal resonances, a phenomena not predictable with linear analysis.

These internal resonances (see Ref. 20) occur as a result of nonlinearities that couple modes of motion (not apparent in the linearized model) and lead to an exchange of energy between the modes of the system as the natural frequencies become commensurable. Such resonances are characterized by periodic amplitude modulation, and the amount of energy that is exchanged depends on the type of nonlinearity and the relationship of the linear natural frequencies. In Ref. 21, response characteristics of a system dynamically similar to Cole's experiment are examined, but these studies are performed in the absence of aerodynamic loads. The results suggest that a two-to-one internal resonance is responsible for the instability because the frequency of the second bending mode is twice the frequency of the first torsional mode. Results show that an antisymmetric vibration mode may be indirectly excited by a two-to-one internal resonance mechanism.

To examine internal resonances in aeroelastic systems, in Ref. 22 a two-degree-of-freedom aeroelastic system is considered. The system is designed such that the integer frequency ratios of 3:1, 2:1, and 1:1 are achieved as the freestream velocity is increased. An internal resonance is observed as evidenced by the growth in response near 3:1 rather than remaining in an LCO as it does at other velocities. The presence of internal resonance in this system suggests a significant number of interesting pathologies within nonlinear aeroelastic systems that should be considered (see Ref. 3).

These previous studies, however, focus on the nonlinear behavior of the uncontrolled nonlinear aeroelastic system, and there is a rather limited set of results on the control of nonlinear aeroelastic systems. Classical multivariable feedback control is applied to a wing section with nonlinear stiffness in Ref. 23. It is established[23] that a linear controller can stabilize the nonlinear system in some circumstances, but the lack of rigorous guarantees of stability is troubling. Moreover, empirical evidence suggests that these control methods can prove unreliable in strongly nonlinear regimes. Active suppression of nonlinear aeroelastic response requires the development of new control strategies appropriate for these nonlinear systems. Note that, to date, the studies have focused either on the nonlinear behavior of the uncontrolled nonlinear aeroelastic system or the implementation of possibly inappropriate linear strategies on the control of nonlinear systems.

A nonlinear controller based on a partial feedback linearization is derived in Ref. 24, and the resulting closed-loop stability is further investigated in Ref. 25. The feedback linearization, however, is critically dependent on the exact cancellation of the nonlinearity. To overcome such a difficulty, Ko et al.[26] introduce a straightforward, linear-in-parameters, adaptive method. Although the theoretical guarantees of stability given in Ref. 26 are satisfying from a theoretical standpoint, a fundamental question remains as to whether the control methods are actually realizable. In this paper, we present experimental results obtained using the adaptive controller introduced in Ref. 26. In particular, the theoretical and experimental responses of a closed-loop system with adaptive partial feedback linearization are presented. We discuss the experimental performance of the method as well as its stability properties.

Nonlinear Aeroelastic System

In this paper, a nonlinear aeroelastic control problem for a two-dimensional wing, as shown in Figs. 1 and 2, is investigated. The wing is mounted on a flexible support that permits two-degree-of-freedom motion. Detailed discussion on the experimental apparatus is presented in a later section of the paper. Denoting h and α as plunge and pitch variables, the equations of motion for this aeroelastic system are obtained as[27]

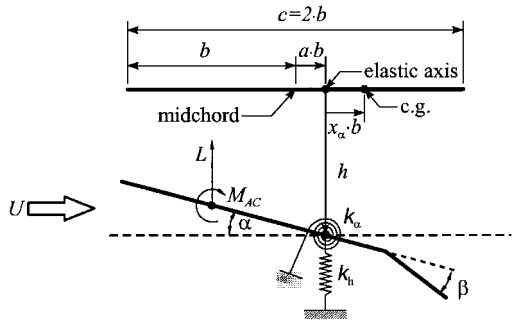

Fig. 1 Aeroelastic model with pitch and plunge degrees of freedom.

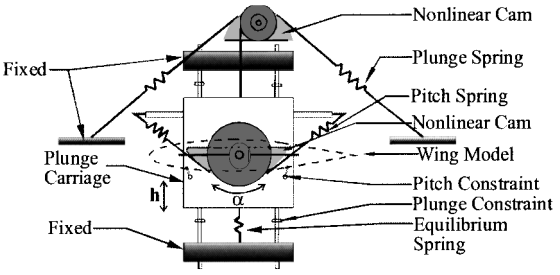

Fig. 2 Schematic view of the experiment setup.

$$\begin{bmatrix} m_T & m_W x_\alpha b \\ m_W x_\alpha b & I_\alpha \end{bmatrix} \begin{Bmatrix} \ddot{h} \\ \ddot{\alpha} \end{Bmatrix} + \begin{bmatrix} c_h & 0 \\ 0 & c_\alpha \end{bmatrix} \begin{Bmatrix} \dot{h} \\ \dot{\alpha} \end{Bmatrix} + \begin{bmatrix} k_h & 0 \\ 0 & k_\alpha(\alpha) \end{bmatrix} \begin{Bmatrix} h \\ \alpha \end{Bmatrix} = \begin{Bmatrix} -L \\ M \end{Bmatrix} \tag{1}$$

where m is the mass of the wing and I_α is the mass moment of inertia about the elastic axis. Note that the total mass of the wing and its support structure is denoted as m_T, and m_W represents the mass of the wing only (see later section on experimental setup). The elastic axis location of the model, a, may be varied for our experiments and plays a significant role in the stability of the system.[24] Conventionally, the elastic axis location a is nondimensionalized with respect to the half-chord length b and is positive for the elastic axis located aft of the midchord. In Eq. (1), x_α is the nondimensionalized distance between the center of mass and elastic axis; c_h and c_α are plunge and pitch structural damping coefficients, respectively; and L and M are the aerodynamic lift and moment about the elastic axis. Structural stiffnesses are k_h and k_α for plunge and pitch motions, respectively. It is possible to incorporate various nonlinear features in this design and the associated experiments. These forms include aerodynamic nonlinear loads, coulomb damping, nonlinear stiffness, higher-order kinematics, etc. However, in this paper, we prescribe the sole source of nonlinearity as a nonlinear torsional stiffness, which is approximated in a polynomial form as

$$k_\alpha(\alpha) = k_{\alpha_0} + k_{\alpha_1}\alpha + k_{\alpha_2}\alpha^2 + k_{\alpha_3}\alpha^3 + k_{\alpha_4}\alpha^4 + \cdots \tag{2}$$

In the experiment, the nonlinear torsional stiffness is realized by nonlinear cams, and the actual coefficients in the preceding polynomial representation are obtained from measured displacement and load measurements.

There are many possible aerodynamic models available to represent the unsteady lift and moment loads. For the purpose of deriving a feedback control for the class of systems discussed in this paper, appropriate choices of unsteady aerodynamic models include the model by Theodorsen and Garrick[28] or a reduced-order model based on frequency-domain analysis. For the development of our adaptive nonlinear controller, we use a quasi-steady aerodynamic model[27]

$$L = \rho U^2 b c_{l_\alpha}\left[\alpha + \dot{h}/U + \left(\tfrac{1}{2} - a\right)b(\dot{\alpha}/U)\right] + \rho U^2 b c_{l_\beta}\beta$$

$$M = \rho U^2 b^2 c_{m_\alpha}\left[\alpha + \dot{h}/U + \left(\tfrac{1}{2} - a\right)b(\dot{\alpha}/U)\right] + \rho U^2 b^2 c_{m_\beta}\beta \tag{3}$$

where U is the freestream velocity and c_{l_α} and c_{m_α} are the aerodynamic lift and moment coefficients. Note that the model is proven appropriate for the low, reduced frequency, subsonic flow that is observed for all of the experiments herein.

The aeroelastic system is controlled by a single trailing-edge flap as shown in Fig. 1, where β represents the flap deflection. For notational simplicity in our subsequent theoretical derivation, we define state variables as

$$\boldsymbol{x} = \begin{Bmatrix} x_1 \\ x_2 \\ x_3 \\ x_4 \end{Bmatrix} = \begin{Bmatrix} h \\ \alpha \\ \dot{h} \\ \dot{\alpha} \end{Bmatrix}$$

Thus, the transformed equations of motion in state-space form become

$$\dot{\boldsymbol{x}} = \boldsymbol{f}(\boldsymbol{x}) + \boldsymbol{g}\beta \tag{4}$$

where

$$\boldsymbol{f}(\boldsymbol{x}) = \begin{Bmatrix} x_3 \\ x_4 \\ -k_1 x_1 - \left[k_2 U^2 + p(x_2)\right] x_2 - c_1 x_3 - c_2 x_4 \\ -k_3 x_1 - \left[k_4 U^2 + q(x_2)\right] x_2 - c_3 x_3 - c_4 x_4 \end{Bmatrix}$$

$$\boldsymbol{g} = \begin{Bmatrix} 0 \\ 0 \\ g_3 \\ g_4 \end{Bmatrix} U^2 \tag{5}$$

The set of new variables introduced in the preceding equations are defined as follows:

$$d = m_T I_\alpha - m_W^2 x_\alpha^2 b^2, \qquad k_1 = I_\alpha k_h / d$$

$$k_2 = \left(I_\alpha \rho b c_{l_\alpha} + m_W x_\alpha \rho b^3 c_{m_\alpha}\right)/d, \qquad k_3 = -m_W x_\alpha b k_h / d$$

$$k_4 = -\left(m_W x_\alpha \rho b^2 c_{l_\alpha} + m_T \rho b^2 c_{m_\alpha}\right)/d$$

$$p(x) = -m_W x_\alpha b k_\alpha(x)/d, \qquad q(x) = m_T k_\alpha(x)/d$$

$$c_1 = \left\{I_\alpha \left(c_h + \rho U b c_{l_\alpha}\right) + m_W x_\alpha \rho U b^3 c_{m_\alpha}\right\}/d$$

$$c_2 = \left\{I_\alpha \rho U b^2 c_{l_\alpha}\left(\tfrac{1}{2} - a\right) - m_W x_\alpha b c_{l_\alpha} + m_W x_\alpha \rho U b^4 c_{m_\alpha}\left(\tfrac{1}{2} - a\right)\right\}/d$$

$$c_3 = \left\{-m_W x_\alpha b \left(c_h + \rho U b c_{l_\alpha}\right) - m_T \rho U b^2 c_{m_\alpha}\right\}/d$$

$$c_4 = \left[m_T \left\{c_\alpha - \rho U b^3 c_{m_\alpha}\left(\tfrac{1}{2} - a\right)\right\} - m_W x_\alpha \rho U b^3 c_{l_\alpha}\left(\tfrac{1}{2} - a\right)\right]/d$$

$$g_3 = -\left(I_\alpha \rho b c_{l_\beta} + m_W x_\alpha b^3 \rho c_{m_\beta}\right)/d$$

$$g_4 = \left(m_W x_\alpha \rho b^2 c_{l_\beta} + m_T \rho b^2 c_{m_\beta}\right)/d$$

As seen from the equations, the nonlinear aeroelastic system is parametrically dependent on the location of the elastic axis a and the freestream velocity U. It is shown in Refs. 24 and 25 that, depending on the values of these parameters, the nonlinear aeroelastic system exhibits a wide variety of bifurcation characteristics.

Active Nonlinear Control

In a series of papers,[24–26] either partial or full feedback linearization has been utilized for the design of a nonlinear controller for the class of aeroelastic systems discussed in this paper. In essence, the feedback linearization seeks to cancel nonlinear dynamics using feedback and then utilizes linear control methodologies for the resulting fully or partially linearized system. Because of its rigorous theoretical foundation in differential geometry, feedback linearization has been employed in a variety of nonlinear control applications including spacecraft attitude control, motor control, and control of wing-rock motion.[29] The detailed theoretical derivation of feedback linearization may be found in Refs. 30 and 31. As the first step of feedback linearization in our application, the output function is simply chosen to be the pitch variable,

$$y(\boldsymbol{x}) = x_2 = \alpha \tag{6}$$

That is, we assume the primary purpose of the control system is to stabilize the pitch motion. The stability of the plunge motion can be deduced by studying the zero dynamics of the partially feedback linearized problem. This topic will be discussed shortly. The plunge variable also can be selected as an output variable in Eq. (6). It has been shown in Ref. 24, however, that the selection of the plunge variable will result in nonlinear zero dynamics in contrast to the linear zero dynamics for the selection of pitch. The resulting nonlinear zero dynamics is shown to exhibit a variety of parametric stability characteristics[25]; thus, the selection of the pitch variable as the output function is preferred.

The preceding choice of output function has a relative degree of 2 via the following simple calculations

$$y(\boldsymbol{x}) = x_2, \qquad L_g y(\boldsymbol{x}) = 0, \qquad L_f y(\boldsymbol{x}) = x_4$$

$$L_g L_f y(\boldsymbol{x}) = g_4 U^2 \neq 0 \tag{7}$$

In Eq. (7). $L_f y$ is the Lie derivative of y in the direction of $\boldsymbol{f}$ and is defined to be

$$L_f y(\boldsymbol{x}) = \sum_i \frac{\partial y}{\partial x_i} f_i \tag{8}$$

Introducing the following state transformation

$$\boldsymbol{x} \mapsto \phi, \qquad \phi_1 = y(\boldsymbol{x}) = x_2, \qquad \phi_2 = L_f y(\boldsymbol{x}) = x_4$$

$$\phi_3 = x_1, \qquad \phi_4 = -g_3 x_4 + g_4 x_3 \tag{9}$$

we obtain an equivalent transformed system:

$$\dot{\phi}_1 = \phi_2, \qquad \dot{\phi}_2 = L_f^2 y(\boldsymbol{x}) + L_g L_f y(\boldsymbol{x})\beta$$

$$\dot{\phi}_3 = A_{32}\phi_2 + A_{34}\phi_4$$

$$\dot{\phi}_4 = [g_3 P_U(\phi_1) - g_4 Q_U(\phi_1)]\phi_1 + A_{42}\phi_2 + A_{43}\phi_3 + A_{44}\phi_4 \tag{10}$$

where

$$L_f^2 y(\boldsymbol{x}) - P_U(\phi_1)\phi_1 - [c_4 + c_3(g_3/g_4)]\phi_2 - k_3\phi_3 - (c_3/g_4)\phi_4$$

$$P_U(\phi_1) = k_4 U^2 + q(\phi_1), \qquad Q_U(\phi_1) = k_2 U^2 + p(\phi_1)$$

$$A_{32} = g_3/g_4, \qquad A_{34} = 1/g_4$$

$$A_{42} = -c_1 g_3 - c_2 g_4 + c_3\left(g_3^2/g_4\right) + c_4 g_3, \qquad A_{43} = k_3 g_3 - k_1 g_4$$

$$A_{44} = c_3(g_3/g_4) - c_1$$

These equations are thereby transformed to the canonical form recognized as amenable to nonlinear geometric control. It is not difficult to show that the given transform and its inverse are well defined for all flow speeds U (see Ref. 24). The partial feedback linearization is then achieved by choosing the feedback control as

$$\beta = \frac{-L_f^2 y(\boldsymbol{x}) + \nu}{L_g L_f y(\boldsymbol{x})} \tag{11}$$

where ν is a new control input. After defining the structure of ν using any linear control methodology, the resulting zero dynamics system is obtained by setting $\phi_1 = \phi_2 = 0$,

$$\begin{Bmatrix} \dot{\phi}_3 \\ \dot{\phi}_4 \end{Bmatrix} = \begin{bmatrix} 0 & A_{34} \\ A_{43} & A_{44} \end{bmatrix} \begin{Bmatrix} \phi_3 \\ \phi_4 \end{Bmatrix} \tag{12}$$

Zero dynamics are defined as the internal dynamics of the partially linearized system. Therefore, the zero dynamics must be stable for

the stability of the entire partially linearized system. As mentioned earlier, the zero dynamics are represented by a set of linear equations; thus, the stability may be checked by investigating the eigenvalues. Figure 3 presents the contour plot of the real part (damping) of the eigenvalues for the aeroelastic system discussed, dependent on the freestream velocity and the elastic axis location. As shown in Fig. 3, the eigenvalues are stable for the ranges of parameters of interest. However, note that the stability of the zero dynamics only guarantees local stability of the closed-loop system.[31]

The preceding feedback linearization is dependent on the exact cancellation of the nonlinearity as shown in Eqs. (10) and (11). When there exist uncertainties in system parameters, however, exact cancellation is not achieved. Thus, the theoretical stability of the closed-loop system may not be realizable for the actual physical system. Two alternatives to address this difficulty include the use of robust or adaptive variants of the geometric control methods. To achieve the closed-loop stability without the exact cancellation as implied in Eqs. (10) and (11), an adaptive methodology is derived in Ref. 26, together with feedback linearization. One source of such uncertainty in our aeroelastic system is the polynomial approximation for the nonlinear torsional stiffness [see Eq. (2)]. To illustrate, Fig. 4 shows the difference between a fifth-order polynomial approximation and the experimentally measured pitch spring stiffness. For the subsequent derivation, it is assumed that the pitch stiffness is represented by an Nth-order polynomial

$$k_\alpha(\alpha) = k_{\alpha_0} + k_{\alpha_1}\alpha + k_{\alpha_2}\alpha^2 + \cdots + k_{\alpha_{N-1}}\alpha^{N-1} \equiv \sum_{i=1}^{N} \theta_i \alpha^{i-1} \tag{13}$$

Note that we have defined $\theta_i = k_{\alpha_{i-1}}$. The adaptive feedback linearization is achieved, first, by expressing the nonlinear term to be canceled in a form such that the uncertain parameters appear linearly, that is, from Eq. (10)

$$L_f^2 y(\boldsymbol{x}) = -P_U(\phi_1)\phi_1 - [c_4 + c_3(g_3/g_4)]\phi_2 - k_3\phi_3 - (c_3/g_4)\phi_4$$

$$\equiv F(\phi) + \sum_{i=1}^{N} \theta_i R_i(\phi) \tag{14}$$

where we define

$$F(\phi) \equiv -k_4 U^2 \phi_1 - [c_4 + c_3(g_3/g_4)]\phi_2 - k_3\phi_3 - (c_3/g_4)\phi_4$$

$$R_i(\phi) \equiv -(m_T/d)\phi_1^i \tag{15}$$

By assuming that the zero dynamics of the feedback linearization are stable, in Ref. 32 it is shown that an adaptive strategy can be derived to handle inexact cancellation of nonlinear terms. Focusing on the subsystem for (ϕ_1, ϕ_2) from Eq. (10), we have

$$\dot{\phi}_1 = \phi_2, \qquad \dot{\phi}_2 = F(\phi) + \sum_{i=1}^{N} \theta_i R_i(\phi) + g_4 U^2 \beta \tag{16}$$

Denoting the estimated values of parameters as $\hat{\theta}_i$, we acheive the certainty equivalent linearization by choosing

$$\beta = \left[-F(\phi) - \sum_i \hat{\theta}_i R_i(\phi) + \nu \right] \Big/ g_4 U^2 \tag{17}$$

Clearly the certainty equivalent control is precisely the partial feedback linearizing control in the event that the estimates $\hat{\theta}_i$ are exact. Substituting the preceding control input into Eq. (16), we obtain

$$\dot{\phi}_1 = \phi_2, \qquad \dot{\phi}_2 = \sum_{i=1}^{N} (\theta_i - \hat{\theta}_i) R_i(\phi) + \nu \equiv (\Theta - \hat{\Theta})^T \boldsymbol{R} + \nu \tag{18}$$

where

$$\Theta = \{\theta_i\}, \qquad \hat{\Theta} = \{\hat{\theta}_i\}, \qquad \boldsymbol{R} = \{R_i(\phi)\} \tag{19}$$

Using any linear feedback control technique, the new input ν is chosen as $\nu = -\bar{k}_1\phi_1 - \bar{k}_2\phi_2$,

$$\begin{Bmatrix} \dot{\phi}_1 \\ \dot{\phi}_2 \end{Bmatrix} = \begin{bmatrix} 0 & 1 \\ -\bar{k}_1 & -\bar{k}_2 \end{bmatrix} \begin{Bmatrix} \phi_1 \\ \phi_2 \end{Bmatrix} + \begin{Bmatrix} 0 \\ \tilde{\Theta}^T \boldsymbol{R} \end{Bmatrix} \tag{20}$$

with estimation error, $\tilde{\Theta} = \Theta - \hat{\Theta}$. Note that $\bar{k}_1, \bar{k}_2$ are determined such that the preceding subsystem is stable when $\Theta = 0$. The evolution equations for the estimation of the parameters $\hat{\Theta}$ are obtained using Lyapunov theory so that the subsystem is asymptotically stable. The Lyapunov function is chosen as

$$V = \frac{1}{2} \begin{Bmatrix} \phi_1 \\ \phi_2 \end{Bmatrix}^T \begin{Bmatrix} \phi_1 \\ \phi_2 \end{Bmatrix} + \frac{1}{2} \tilde{\Theta}^T \tilde{\Theta} \tag{21}$$

The derivative along the system trajectory is obtained by differentiating, and we find

$$\dot{V} = \begin{Bmatrix} \phi_1 \\ \phi_2 \end{Bmatrix}^T \bar{A} \begin{Bmatrix} \phi_1 \\ \phi_2 \end{Bmatrix} + \phi_2 \tilde{\Theta}^T \boldsymbol{R} + \tilde{\Theta}^T \dot{\tilde{\Theta}} \tag{22}$$

where

$$\bar{A} = \begin{bmatrix} 0 & 1 \\ -\bar{k}_1 & -\bar{k}_2 \end{bmatrix}$$

Note that by choosing

$$-\dot{\tilde{\Theta}} (= \dot{\hat{\Theta}}) = \phi_2 \boldsymbol{R} \tag{23}$$

we have $\dot{V} \leq 0$ because $\bar{A}$ is constructed to be negative definite. It is emphasized that the convergence of the parameters is not guaranteed, nor is it necessary. The stability of the system (towards the level sets of $\dot{V} = 0$) is guaranteed by the invariant manifold theorem of La Salle and Lefschetz.[33]

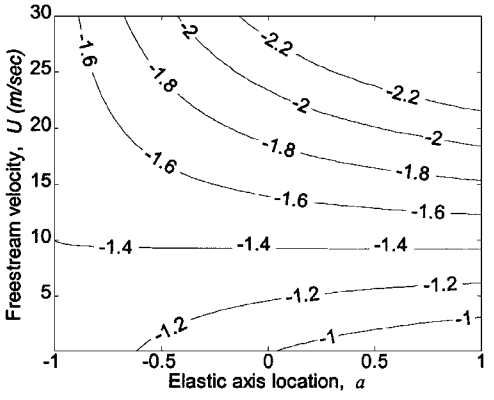

Fig. 3 Contour plot of the real part of the eigenvalues for the zero dynamics.

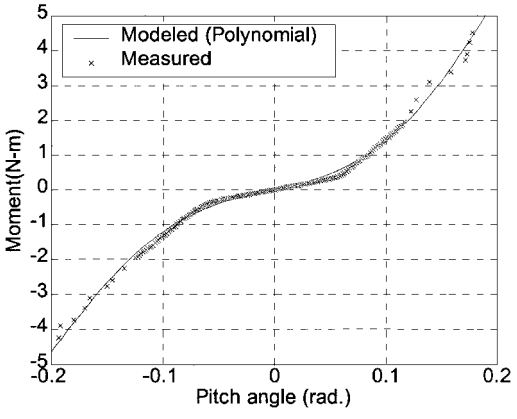

Fig. 4 Measured and modeled moment vs pitch angle for nonlinear pitch spring.

Experimental Setup

In this section we describe the experimental system that serves as the testbed for experimental investigations and validation of the numerical predictions of the adaptive control strategy. A model support system (see Fig. 2) has been developed to provide direct measurements[16] of nonlinear aeroelastic response as well as examine new control strategies of such response.[23] A detailed description of the test apparatus is presented in Ref. 23. The support system permits prescribed pitch and plunge motion for a mounted wing section. For studies of control of nonlinear aeroelastic response, the wing includes a full-span trailing-edge flap. The plunge degree of freedom is provided by a carriage that translates. Pitch motion, independent of plunge motion, is provided by rotational cams that are mounted on this carriage.

Large AOA are permitted, but protective constraints limit the amplitude of motion to prevent model/tunnel damage from large amplitude LCOs or flutter. These constraints do not affect the onset of flutter. Typically, only the mass of the wing is considered in analysis; however, because the carriage moves with the attached wing, the mass of both the wing model and support structure must be considered in the analysis. In addition, the moment of inertia associated with the pitch motion does not include a contribution from the carriage mass because this portion of the system does not pitch. These details are reflected in the equations of motion [Eq. (1)].

The model support system provides freedom in test conditions and parameters. The structural stiffness response of the apparatus is governed by a pair of cams that are designed to provide tailored linear or nonlinear stiffness response. The shape of each cam, stiffness of the springs, and pretension in the springs dictate the nature of the nonlinearity. With this approach, these cams provide a large family of prescribed responses. Other physical properties, such as the eccentricity of the aerodynamic center, the mass of various system components, the mass eccentricity, the moment of inertia of the wing, the stiffness characteristics, and the wing shape, are easily modified for parametric investigations. This configuration also permits studies of internal resonances such as those presented in Ref. 22.

System response is measured with accelerometers and optical encoders mounted to track motion in each degree of freedom. The plunge and pitch displacements are measured with optical encoders attached to shafts running through the respective cams. The plunge and pitch accelerations are measured with accelerometers. Freestream velocity is determined from a pitot probe mounted in the test section.

To ensure sufficient data acquisition speed, a dual acquisition process is used. First, the digital optical encoders are read by a (Data Translation DT2821-F-16SE) data acquisition board in conjunction with a custom electronics board. A custom computer program converts the digital readings to analog outputs. A second personal computer samples these analog optical encoder signals, along with the analog outputs from the accelerometers and the pitot tube pressure transducer. This primary data acquisition computer uses a National Instruments PCI-MIO-16XE-10 data acquisition board. Custom software developed in the LabVIEW environment from National Instruments allows the data to be sampled and recorded, with real-time calculation of all parameters. This software also provides active control commands. Control laws are developed independently as dynamic-link libraries and then integrated into the control software. A detailed input/output data flow diagram for the measurement and control setup is presented in Fig. 5.

Experiments are conducted by setting the freestream velocity and initial conditions, releasing the structure, and measuring the response. Initial conditions are set by dictating both a pitch and plunge initial condition, or by dictating a pitch condition and allowing the plunge response to displace freely. The initial conditions are displacements; no initial velocities are used. The accelerations are acquired using an analog to digital board, and the frequency content of the measurements are analyzed using fast Fourier transform techniques. The optical encoders require digital input/output boards and output storage. Measurements are examined to determine frequency, damping, and other stability characteristics prior to increasing the freestream velocity to the next test point. Flutter is determined by monitoring the frequency and damping of the measured motion, as well as observation of the system response.

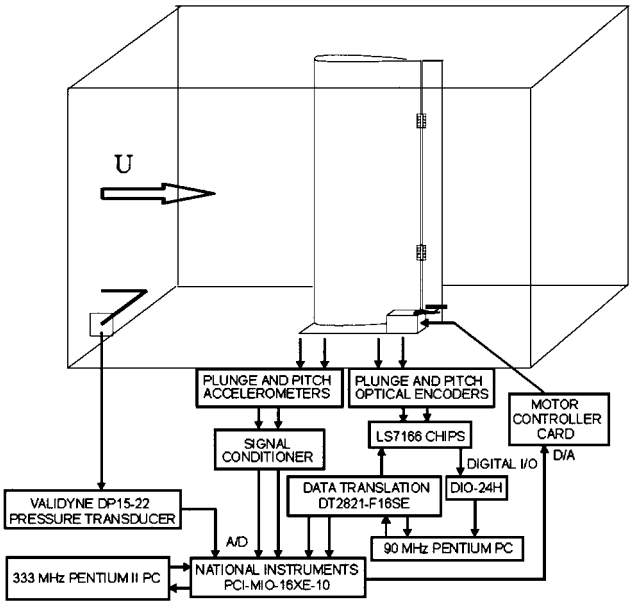

Fig. 5 Schematic of data input/output for measurements and control of experiments.

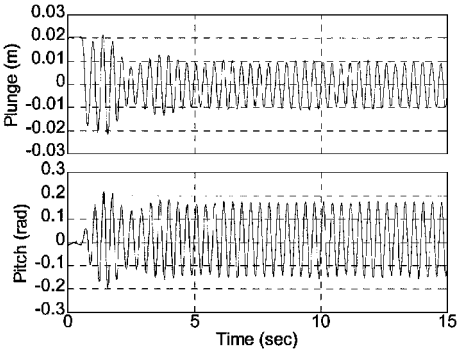

Fig. 6 Measured open-loop responses of pitch and plunge at U = 16 m/s.

Results and Discussion

For the construction of the feedback control for the aeroelastic system discussed, the nonlinear pitch spring stiffness is measured, and the fifth-order polynomial approximation of the stiffness is obtained as

$$k_\alpha(\alpha) = 6.833 + 9.967\alpha + 667.685\alpha^2 + 26.569\alpha^3 - 5087.931\alpha^4 \ (\mathrm{N \cdot m/rad}) \tag{24}$$

Measurements of moment vs pitch angle are compared to this approximated stiffness in Fig. 4. We note that a small difference between measured and approximated stiffness exists and, as a consequence, presents an uncertainty that exercises the adaptive control.

For an initial plunge displacement of $h = 0.02$ m, the measured open-loop responses of the plunge and pitch displacements, for a freestream velocity of $U = 16$ m/s, are shown in Fig. 6. Clearly the system responses exhibit LCO behavior. A thorough investigation of the existence of LCO with various initial conditions and freestream velocities for this experimental apparatus may be found in Ref. 16. The existence of LCO is dependent on the initial displacement and the freestream velocities, but in general LCO occurs for freestream velocities larger than 13 m/s (Ref. 16) for this configuration. Figure 7 presents the simulated responses at the same freestream velocity. Note that the use of the quasi-steady aerodynamic model in our analytical analysis provides excellent agreement between measured and simulated responses in terms of the magnitudes and the frequencies of the LCO. Also note that the frequency associated with the

Table 1 System parameters

Parameter	Value
m_T	12.3870 kg
m_W	2.0490 kg
b	0.135 m
ρ	1.225 kg/m^3
x_α	$[0.0873 - (b + ab)]/b$ m
I_α	$m_W x_\alpha^2 b^2 + 0.0517$ kg · m^2
Span	0.6 m
c_{l_α}	6.28
c_{l_β}	3.358
c_{m_α}	$(0.5 + a)c_{l_\alpha}$
c_{m_β}	−1.94
k_h	2844.4 N/m
$k_\alpha(\alpha)$	See Eq. (24)
c_h	27.43 kg/s
c_α	0.036 kg m^2/s
a	−0.6847

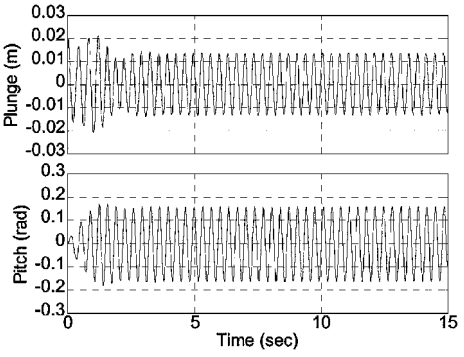

Fig. 7 Predicted open-loop responses of pitch and plunge at U = 16 m/s.

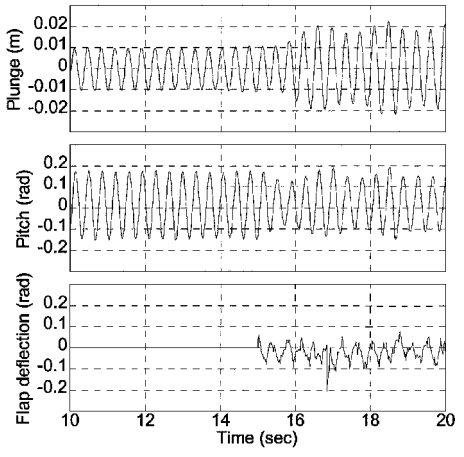

Fig. 8 Measured closed-loop responses at U = 16 m/s for the linear controller constructed in Ref. 23.

simulated responses is slightly higher than the measured responses due to the presence of unmodeled aerodynamic lag (damping) in the experiment. The physical parameters of the experimental apparatus, which are used for the numerical simulation, are given in Table 1.

Encouraged by good correlation between simulated and measured responses of the open-loop aeroelastic system, the nonlinear adaptive controller derived herein is implemented and tested by experiment. In the experiments, an initial disturbance is introduced that leads to LCO, and then the controller is activated at a predetermined time ($t = 15$ s). A typical response using the classical multivarible linear controller constructed in Ref. 23 is shown in Fig. 8. We emphasize that in some cases the controller is able to stop the LCO after a period of rather large, transient oscillations, but in general

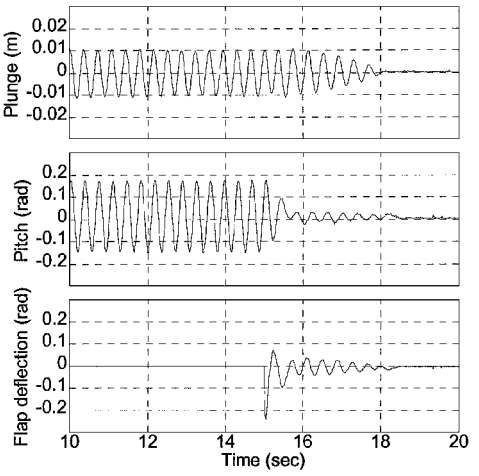

Fig. 9 Measured closed-loop responses at U = 16 m/s for the adaptive feedback linearization.

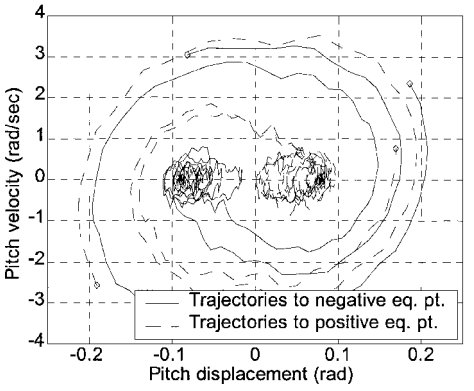

Fig. 10 Phase portrait of closed-loop responses (pitch degree of freedom) for feedback linearization without adaptive feedback control.

the closed-loop responses are unpredictable. Note, however, that in Ref. 23 it is shown that the linear controller derived in Ref. 23 is able to stabilize the nonlinear system if the controller is started before the system is entrained in LCO. Control was not always possible using the linear approach. On the other hand, the adaptive controller derived herein is able to stabilize the LCO up to 23% above the nominal flutter velocity. Figure 9 is the response observed for the adaptive controller at the freestream velocity $U = 16$ m/s. The adaptive controller is unable to stabilize the LCO at higher freestream velocities (above 17 m/s), but notable improvements are realizable using the nonlinear model. Recall that the closed-loop stability of the modeled aeroelastic system is guaranteed independent of freestream velocities. However, inevitable modeling errors make this ideal adaptive control unrealizable for higher velocities. Thus, an improvement to the current controller may be achieved by incorporating a better aerodynamic model or structural torsional stiffness model.

An interesting observation is made when a controller based on feedback linearization without adaptivity is employed as an active control. Specifically, when the controller is activated, the closed-loop system trajectories converge to either one of two nonzero equilibrium points, rather than to the trivial zero equilibrium point. Measurements from several cases at $U = 16$ m/s are collected for the construction of phase portraits and are shown in Fig. 10 for the pitch degree of freedom. In Fig. 10, trajectories converge either to negative equilibrium or to positive equilibrium as shown. The phase portrait is very similar to that presented in Ref. 24 for the case in which two stable and one saddle equilibrium points are present. This observation validates the importance of adaptation in the design of nonlinear control system, especially for the feedback linearization discussed in this paper, as the exact characterization of nonlinearities is often difficult to achieve.

Conclusion

Nonlinearities may significantly affect the aeroelastic stability of certain aircraft configurations, and these nonlinearities must be considered for the accurate prediction and active suppression of associated instabilities. In this paper, the authors present the derivation of nonlinear control strategies for active suppression of LCOs in a wing section with structural nonlinearity and also present related experimental results obtained in wind tunnel. Specifically, measured open-loop responses are shown, and clearly the system responses exhibit LCO behavior. The use of a quasi-steady aerodynamic model (appropriate for the low, reduced frequency of the experiments) provides excellent agreement between measured and simulated responses in terms of the magnitudes and the frequencies of the LCOs.

Most previous studies focus on the nonlinear behavior of the uncontrolled nonlinear aeroelastic system. Whereas some studies do exist that address control of the nonlinear system, these typically implement linear strategies that may prove inadequate. The authors suggest that active suppression of nonlinear aeroelastic response requires the development of new control strategies appropriate for these nonlinear systems. Although the classical multivarible linear controller may suppress the LCO for some cases, it is shown that the closed-loop responses are unpredictable and control is not always possible using the linear approach. A nonlinear controller based on a partial feedback linearization approach is derived, and the resulting closed-loop stability is investigated. Experimental results show that feedback linearization is critically dependent on the exact cancellation of the nonlinearity. This observation validates the importance of adaptation in the design of the nonlinear control system because the exact characterization of nonlinearities is often difficult.

Thus, a nonlinear adaptive controller with validation by experiment is presented. Notable improvements are realized using the nonlinear model as the adaptive controller stabilizes the LCO.

References

[1]Denegri, C. M., and Cutchins, M. A., "Evaluation of Classical Flutter Analyses for the Prediction of Limit Cycle Oscillations," AIAA Paper 97-1021, Structures, Structural Dynamics, and Materials Conference, AIAA, Reston, VA, April 1997.

[2]Chen, P., Sarhaddi, D., and Liu, D., "Limit-Cycle-Oscillation Studies of a Fighter with External Stores," AIAA Paper 98-1727, *Structures, Structural Dynamics, and Materials Conference*, AIAA, Reston, VA, April 1998.

[3]Stearman, R. O., Powers, E. J., Schwartz, J., and Yurkovich, R., "Aeroelastic Identification of Advanced Technology Aircraft Through Higher Order Signal Processing," *Proceedings of the 9th International Modal Analysis Conference*, Society for Experimental Mechanics, Bethel, CT, 1991, pp. 1607–1616.

[4]Dowell, E. H., "Nonlinear Aeroelasticity," AIAA Paper 90-1031, *Structures, Structural Dynamics, and Materials Conference*, AIAA, Washington, DC, April 1990.

[5]Dowell, E. H., and Ilgamov, M., *Studies in Nonlinear Aeroelasticity*, Springer–Verlag, New York, 1988, pp. 163–205.

[6]Lee, B. H. K., Price, S. J., and Wong, Y. S.,"Nonlinear Aeroelastic Analysis of Airfoils: Bifurcation and Chaos," *Progress in Aerospace Sciences*, Vol. 35, No. 3, 1999, pp. 205–334.

[7]Conner, M. D., Tang, D. M., Dowell, E. H., and Virgin, L. N., "Nonlinear Behavior of a Typical Airfoil Section with Control Surface Freeplay: A Numerical and Experimental Study," *Journal of Fluids and Structures*, Vol. 11, No. 1, 1997, pp. 89–109.

[8]Price, S. J., Alighanbari, H., and Lee, B. H. K., "The Aeroelastic Response of a Two-Dimensional Airfoil with Bilinear and Cubic Structural Nonlinearities," *Journal of Fluids and Structures*, Vol. 9, No. 2, 1995, pp. 175–193.

[9]Price, S. J., Lee, B. H. K., and Alighanbari, H., "Postinstability Behavior of a Two-Dimensional Airfoil with a Structural Nonlinearity," *Journal of Aircraft*, Vol. 31, No. 6, 1994, pp. 1395–1401.

[10]Alighanbari, H., and Price, S. J., "The Post-Hopf-Bifurcation Response of an Airfoil in Incompressible Two-Dimensional Flow," *Nonlinear Dynamics*, Vol. 10, No. 4, 1996, pp. 381–400.

[11]Tang, D. M., and Dowell, E. H., "Flutter and Stall Response of a Helicopter Blade with Structural Nonlinearity,"*Journal of Aircraft*, Vol. 29, No. 5, 1992, pp. 953–960.

[12]Tang, D. M., and Dowell, E. H., "Comparison of Theory and Experiment for Non-Linear Flutter and Stall Response of a Helicopter Blade," *Journal of Sound and Vibration*, Vol. 165, No. 2, 1993, pp. 251–276.

[13]Woolston, D. S., Runyan, H. L., and Andrews, R. E., "An Investigation of Effects of Certain Types of Structural Nonlinearities on Wing and Control Surface Flutter," *Journal of the Aeronautical Sciences*, Vol. 24, No. 1, 1957, pp. 57–63.

[14]Lee, B. H. K., and LeBlanc, P., "Flutter Analysis of a Two-Dimensional Airfoil with Cubic Nonlinear Restoring Force," National Aeronautical Establishment, Aeronautical Note 36, National Research Council 25438, Ottawa, ON, Canada, Feb. 1986.

[15]Zhao, L. C., and Yang, Z. C., "Chaotic Motions of an Airfoil with Nonlinear Stiffness in Incompressible Flow," *Journal of Sound and Vibration*, Vol. 138, No. 2, 1990, pp. 245–254.

[16]O'Neil, T., and Strganac, T. W., "Aeroelastic Response of a Rigid Wing Supported by Nonlinear Springs," *Journal of Aircraft*, Vol. 35, No. 4, 1998, pp. 616–622.

[17]Lee, B. H. K., Gong, L., and Wong, Y. S., "Analysis and Computation of Nonlinear Dynamic Response of a Two-Degree-of-Freedom System and Its Application in Aeroelasticity," *Journal of Fluids and Structures*, Vol. 11, No. 3, 1997, pp. 225–246.

[18]Lee, B. H. K., Jiang, L. Y., and Wong, Y. S., "Flutter of an Airfoil with a Cubic Restoring Force," AIAA Paper 98-1725, *Structures, Structural Dynamics, and Materials Conference*, AIAA, Reston, VA, April 1998.

[19]Cole, S. R., "Effects of Spoiler Surfaces on the Aeroelastic Behavior of a Low-Aspect Ratio Wing," AIAA Paper 90-0981, *Structures, Structural Dynamics, and Materials Conference*, AIAA, Washington, DC, April 1990.

[20]Nayfeh, A. H., and Mook, D. T., *Nonlinear Oscillations*, Wiley, New York, 1979, pp. 1–70.

[21]Oh, K., Nayfeh, A. H., and Mook, D. T., "Modal Interactions in the Forced Vibration of a Cantilever Metallic Plate," *Nonlinear and Stochastic Dynamics*, edited by A. K. Bajaj, N. S. Namachchiraya, and R. A. Ibrahim, Vol. 78, American Society of Mechanical Engineers, Fairfield, NJ, 1994, pp. 237–247.

[22]Gilliatt, H. C., Strganac, T. W., and Kurdila, A. J., "On the Presence of Internal Resonances in Aeroelastic Systems," AIAA Paper 98-1955, *Structures, Structural Dynamics, and Materials Conference*, AIAA, Reston, VA, April 1998.

[23]Block, J. J., and Strganac, T. W., "Applied Active Control for a Nonlinear Aeroelastic Structure," *Journal of Guidance, Control, and Dynamics*, Vol. 21, No. 6, 1999, pp. 838–845.

[24]Ko, J., Kurdila, A. J., and Strganac, T. W., "Nonlinear Control of a Prototypical Wing Section with Torsional Nonlinearity," *Journal of Guidance, Control, and Dynamics*, Vol. 20, No. 6, 1997, pp. 1181–1189.

[25]Ko, J., Strganac, T. W., and Kurdila, A. J., "Stability and Control of a Structurally Nonlinear Aeroelastic System," *Journal of Guidance, Control, and Dynamics*, Vol. 21, No. 5, 1998, pp. 718–725.

[26]Ko, J., Strganac, T. W., and Kurdila, A. J., "Adaptive Feedback Linearization for the Control of a Typical Wing Section with Structural Nonlinearity," *Nonlinear Dynamics*, Vol. 18, No. 3, 1999, pp. 289–301.

[27]Fung, Y. C., *An Introduction to the Theory of Aeroelasticity*, Wiley, New York, 1955, pp. 207–215.

[28]Theodorsen, T., and Garrick, I. E., "Mechanism of Flutter: A Theoretical and Experimental Investigation of the Flutter Problem," NACA Rept. 685, 1940.

[29]Monahemi, M. M., and Krstic, M., "Control of Wing Rock Motion Using Adaptive Feedback Linearization," *Journal of Guidance, Control, and Dynamics*, Vol. 19, No. 4, 1996, pp. 905–912.

[30]Isidori, A., *Nonlinear Control Systems*, Springer–Verlag, New York, 1989, pp. 1–82.

[31]Slotine, J. E., and Li, W., *Applied Nonlinear Control*, Prentice–Hall, Englewood Cliffs, NJ, 1991, pp. 207–275.

[32]Sastry, S. S., and Isidori, A., "Adaptive Control of Linearizable Systems," *IEEE Transactions on Automatic Control*, Vol. 34, No. 11, 1989, pp. 1123–1131.

[33]La Salle, J., and Lefschetz, S., *Stability by Liapunov's Direct Method*, Academic Press, New York, 1961, pp. 56–71.